# Wave functions with localizations on classical periodic orbits in weakly perturbed quantum billiards

C. C. Liu,* T. H. Lu, Y. F. Chen, and K. F. Huang

*Department of Electrophysics, National Chiao Tung University, 1001 Ta Hsueh Road, Hsinchu, 30050 Taiwan*

We analytically investigate quantum wave functions with localizations on classical periodic orbits (POs) in the circular billiards. We construct the coherent states which are the coherent superpositions of nearly degenerate eigenstates and found to be localized around single classical POs. With the constructed coherent states, we can analytically express the mesoscopic eigenstates in the weakly perturbed systems, which are found to be localized on the ensemble of classical POs. Furthermore, these coherent states can be utilized to study the quantum vortex structures in quantum billiards.

PACS number(s): 05.45.Mt, 03.65.Ge, 03.65.Vf, 67.40.Vs

## I. INTRODUCTION

The exploration of the mesoscopic billiard is one of the most useful tools for connecting quantum mechanics with the classical limit. For two-dimensional billiards, the simpler shapes include the triangle, the square, and the circle. The circular billiard could be regarded as the $N$-sided regular polygon with $N \to \infty$. In other words, the circular billiard has the highest symmetry in the angular coordinate $\phi$ and its trajectories have a one-dimensional degeneracy corresponding to the rotational symmetry of the system. The interplay between the classical *periodic orbits* (POs) and the quantum energy spectrum has been extensively discussed in the circular billiard [1–5]. Furthermore, the weakly perturbed circular billiards are often used to study the transitions of wave functions from regular to chaotic distributions [6–11]. The wave functions with localizations on classical POs conspicuously emerge in Lee *et al.*'s numerical eigenstates of the perturbed system in the index-guided circular microcavity with the spiral-shape deformation [12]. Earlier, Chinnery *et al.* built an acoustic apparatus to visualize the wave patterns in a water-filled circular cavity [13]. They found that the resonant patterns are Bessel-like eigenstates in the low-order regime; however, wave patterns localized on POs usually appear in the high-order regime. There are several optical experiments for the weakly perturbed circular cavity to explore the characteristics of the wave patterns [14–17]. Their results also reveal that the weak deformation on the regular shape often causes the resonant wave patterns concentrated on classical POs. Therefore, the classical POs play a crucial role in the eigenstates of the deformed mesoscopic quantum system. Even so, the relationship between the classical POs and the mesoscopic wave functions has not been clearly explored as yet for the weakly perturbed quantum system.

Here we use the correspondence between classical dynamics and quantum spectra to construct the coherent states (CSs) associated with single classical POs. The constructed CSs are further employed to represent the eigenstates in the weakly perturbed systems in a manifest way, in which the mesoscopic eigenstates are usually localized on the ensemble of the classical POs. The analytic connection between per-

turbed eigenstates and CSs reveals the significance of the relative phase in quantum-classical transition. Finally, we utilize these CSs to study the vortex structures of the mesoscopic wave functions in quantum vector currents. Vortices are responsible for many observed phenomena known mainly to occur in macroscopic quantum systems, such as superconductors or superfluids [18]. In recent years, there has been growing attention to the occurrence of quantum vortices in the current flow of mesoscopic structures especially in semiconductor open quantum dots [19], in which the ballistic quantum transport reveals that the quantum states associated with the classical POs play an important role in the striking phenomena of conductance fluctuations.

## II. COHERENT STATES WITH LOCALIZATIONS ON SINGLE CLASSICAL PERIODIC ORBITS

Periodic orbits in classical circular billiards are defined by two parameters $(p, q)$. The value of $p$ is the number of bouncing points on the boundary of a closed trajectory, and the value of $q$ is determined by the chord angle of the successive bounces. As shown in Figs. 1(a) and 1(b), the $p$-bouncing points divide the circumferential angle into $p$ parts of $2\pi/p$, and the chord angle $\Theta$ is equal to the product of $q$ and $2\pi/p$, i.e., $\Theta = q \cdot 2\pi/p$. Besides, the initial point of the classical PO is described by angle $\theta_{PO}$ as shown in Figs. 1(c) and 1(d), where $\theta_{PO}$ is the included angle between horizontal and the intercept $\overline{OT}$ and increases as $\overline{OT}$ rotates in the counterclockwise direction.

In classical dynamics, as shown in Fig. 1(b), the radial-component velocity related to the center $O$ at the turning point $T$ vanishes leaving only angular-component velocity. All energy turns into angular energy under the conservation of energy, i.e., the energy at point $T$ is given by

$$E = \frac{L_{max}^2}{2\mu R_{min}^2} = \frac{L_{max}^2}{2\mu \left[ R \cos\left(\frac{\Theta}{2}\right) \right]^2}, \quad (1)$$

with $R_{min} \equiv \overline{OT} = R \cos\left(\frac{\Theta}{2}\right)$. In quantum mechanics, the solutions of Schrödinger equation for a circular billiard satisfied the Dirichlet boundary condition are

$$\psi_{n,\ell}(r, \phi) = J_\ell(k_{n,\ell} r) e^{i\ell\phi}, \quad (2)$$

where $\ell$ and $n$ are the angular and radial quantum numbers, respectively, and $k_{n,\ell}$ is the wave number of the $n$th zero of
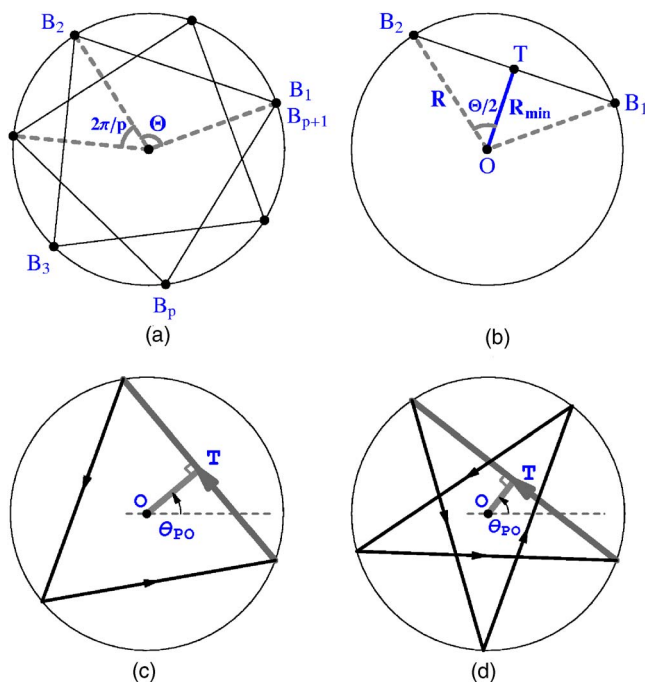
FIG. 1. (Color online) Classical $(p,q)$ PO motions: (a) The $p$-bouncing points at boundary divide the circumference into each angle being $2\pi/p$. (b) The chord angle of successive bouncing is $\Theta = q \cdot 2\pi/p$. (c), (d) The angle $\theta_{\mathrm{PO}}$ is defined for (3, 1) and (5, 2) POs.

$\ell$th Bessel function $J_\ell(k_{n,\ell} r)$. Here the angular component $e^{i\ell\phi}$ is in the form of traveling wave, while substituting by $\cos(\ell\phi)$ or $\sin(\ell\phi)$ it is in the form of standing wave. In the following, if not mentioned, the wave functions used are the complex wave functions, i.e., the traveling waves. The quantized energy and angular momentum are given by

$$E = \frac{\hbar^2 k_{n,\ell}^2}{2\mu} \quad \text{and} \quad L_z = \ell \, \hbar \,, \qquad (3)$$

respectively, where the constant $\hbar$ and particle mass $\mu$ will be set to be unit.

Under the classical limit, the semiclassical wave number can be obtained from Eqs. (1) and (3) and $\Theta = q \cdot 2\pi/p$ as [5]

$$k_{\mathrm{sc}}(p,q,\ell) = \frac{\ell}{R \cos\left(\frac{q\pi}{p}\right)}. \qquad (4)$$

The value of $k_{\mathrm{sc}}(p,q,\ell)$ for a motion of $(p,q)$ PO is determined if we give the angular number $\ell$, for instance, $k_{\mathrm{sc}}(3,1,100)=200.0$, $k_{\mathrm{sc}}(4,1,100)=141.4$, and $k_{\mathrm{sc}}(5,2,100)=323.6$. In Fig. 2, we draw three horizontal lines with values of $k_{\mathrm{sc}}(3,1,100)$, $k_{\mathrm{sc}}(4,1,100)$, and $k_{\mathrm{sc}}(5,2,100)$. According to these three horizontal lines, $\ulcorner \times \lrcorner$ points, which have the nearest distance from the horizontal lines, are selected from numerous open-symbol points $(k_{n,\ell}, \ell, n)$. These selected $\ulcorner \times \lrcorner$ points are nearly degenerate eigenstates and their angular numbers $\ell(K)$ and nodal numbers $n(K)$ have the formulas

$$\ell(K) = \ell(0) \pm K \cdot p, \qquad (5)$$

$$n(K) = n(0) \mp K \cdot q, \qquad (6)$$

with $K = 0, 1, 2, \ldots, N$. For a given $\ell(0)$, $N$ can be determined by the constraint of difference between $k_{n,\ell}$ and $k_{\mathrm{sc}}$, i.e., $\Delta k = k_{n,\ell} - k_{\mathrm{sc}}$. Here, the jump of $p$ in $\ell(K)$ is based on the $p$ degeneracy in the angular part of the wave function, $e^{i\ell\phi}$, and the multiple of $q$ in the corresponding $n(K)$ is given from the $n$ values of the dashed lines. As a consequence, these nearly degenerate eigenstates have a relationship between the quantum numbers of eigenstates and the parameters of PO: $(\Delta\ell, \Delta n) = (\pm p, \mp q)$, and the horizontal lines with values of $k_{\mathrm{sc}}(p,q,\ell)$ are the references of picking the nearly degenerate eigenstates $\ulcorner \times \lrcorner$.

It is well known that Schrödinger in 1926 [20] originally constructed a CS of a one-dimensional harmonic oscillator to describe a classical particle with a wave packet whose center in the time evolution follows the corresponding classical motion. Extended to the two-dimensional system, the Schrödinger CS is expected to correspond to a wave packet with its center generally moving along a classical trajectory. This exact correspondence enables one to derive the stationary CSs related to the classical Lissajous orbits form the time-dependent Schrödinger CSs [21].

In quantum billiards, the stationary CSs corresponding to the classical motion have been analytically constructed for square and triangular billiards by using the presentation of the SU(2) CSs and obtain well localization on the corresponding classical POs [22,23]. For circular billiards, with the nearly degenerate eigenstates stated in Eqs. (5) and (6), the wave functions associated with single $(p,q)$ POs can be represented by the CSs

$$\Psi_{N,\ell(0)}^{p,q}(r,\phi;\theta) = 2^{-N} \sum_{K=-N}^{N} \binom{2N}{N+K}^{1/2} e^{\pm iK\cdot\theta}$$

$$\times \psi_{n(0)-K\cdot q,\ell(0)+K\cdot p}(r,\phi), \qquad (7)$$

where $e^{\pm iK\cdot\theta}$ is the relative phase between various components of the eigenstates $\psi_{n(0)-K\cdot q,\ell(0)+K\cdot p}$ in Eq. (2). By varying the angle $\theta$, one can find that the relationship between $\theta$ and $\theta_{\mathrm{PO}}$ can be given as $\theta_{\mathrm{PO}} = \theta/p$. Consequently, the relative phase factor is relative to initial points of classical PO. Because of the symmetry, for different phase factors, the localized POs in the circular billiard only rotate their orientations but do not change their shapes, while in the triangular or rectangular billiard the geometric shapes of localized POs are changed [22,23]. Therefore, the phase factor plays an important role in the quantum-classical connection, which has also been confirmed in the studies of the harmonic oscillator, the square billiard, and the triangular billiard and demonstrated by experiments [21–25].

To analyze the constructed CSs in Eq. (7) and realize their connection with classical motion of a particle in billiard, we compute the phase space distributions of the constructed CSs by Poincaré Husimi functions. Figures 3(a) and 3(b) display the CSs and the corresponding Poincaré Husimi functions in the forms of standing and traveling waves, $\cos(\ell\phi)$ and $e^{i\ell\phi}$, respectively. Where $s$ is labeled a point on the boundary ($0 \leq s < 1$) and $\chi$ is the angle of incidence with respect to the
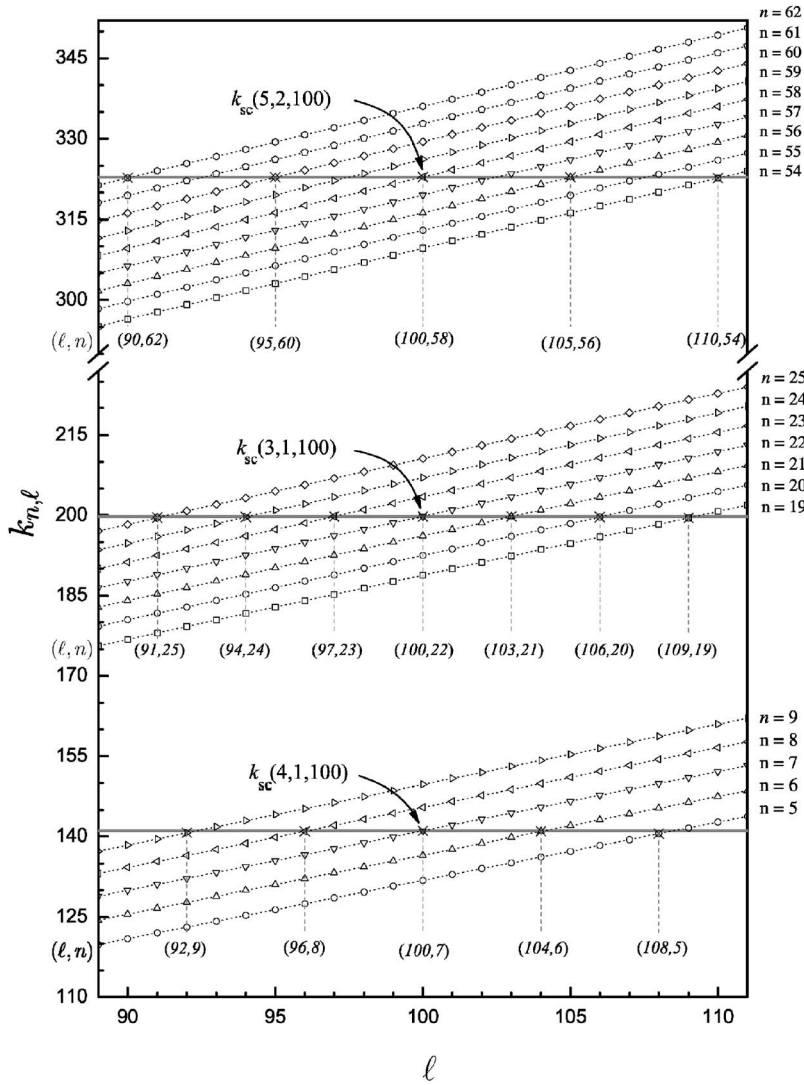
FIG. 2. The nearly degenerate eigenstates. The symbol $\ulcorner \times \lrcorner$ is marked for the nearly degenerate states, which are picked from numerous states $(k_{n,\ell}, \ell, n)$ and have the nearest distance from the horizontal lines. The values of the horizontal lines are determined by connecting classical dynamics and quantum mechanics as Eq. (4).

outward boundary normal at $s$, as shown in Fig. 3(c). It is clear that CS in the form of standing wave is related to the particle incident in both positive and negative directions (counterclockwise and clockwise) with $\chi = \pm 30°$, while CS in the form of traveling wave is related to particle incident only in the positive direction.

Although the number of eigenstates used in the CS $\Psi^{p,q}_{N,\ell(0)}(r, \phi; \theta)$ is $2N+1$, the number of dominant eigenstates for wave localization is rather small, not larger than $\sqrt{\ell(0)}$, for high-order states [21]. The CSs $\Psi^{p,q}_{N,\ell(0)}(r, \phi; \theta)$ can be modified to be partially CSs

$$\Psi^{p,q}_{M,\ell(0)}(r, \phi; \theta) = \sum_{K=-M}^{M} e^{\pm iK\theta} \psi_{n(0)-K \cdot q, \ell(0)+K \cdot p}(r, \phi), \quad (8)$$

in which the weight for each componential eigenstate can be regarded as constant and is set to be unit. It is interesting to point out that the sign of the angular number is opposite to the sign of the nodal number in the subscript of Eq. (8). They are originally obtained from the deriving of the nearly degenerate eigenstates and can be recognized that the simultaneous changes of increasing $\ell(K)$ and decreasing $n(K)$ are to

keep the energies of the eigenstates to be (nearly) constant. Consistently, the same behaviors happen to the quantum numbers studied in the Cartesian systems [22,23].

Since the components of the CSs in Eq. (8) are not exactly degenerate for the Hamiltonian $H$, the partially CSs in Eq. (8) are not stationary states for a perfect circular billiard. Although a quantitative method is not developed to estimate the closeness of the eigenstates, a qualitative analysis can be given as follows. To manifest the efficiency of wave localization, one would need the approval of $\Delta E / \langle E \rangle \rightarrow 0$ by the superposing number $2M+1$ and the quantum number $\ell(0)$ being sufficiently large so that one can ensure the CSs being stationary states in the classical limit. Here $\langle E \rangle$ is the expectation value of the Hamiltonian and $\Delta E$ is the dispersion in energy $\langle |E - \langle E \rangle| \rangle$. We show several patterns superposed with $2M+1 = 3, 5, 7$, and 9 in the right-up inset of Fig. 4. It is apparent that the needed number of superposed eigenstates for the CS with clearly localized POs is rather small. Only five nearly degenerate eigenstates are sufficient to construct the CS. The effect of the angular quantum number $\ell(0)$ on the localized patterns is also shown in Fig. 4. The solid line depicts $\langle |E - \langle E \rangle| \rangle / \langle E \rangle$ related to $\ell(0)$ and the open circles are marked at $\ell(0) = 20, 35, 60, 120$, and 180 accompanying
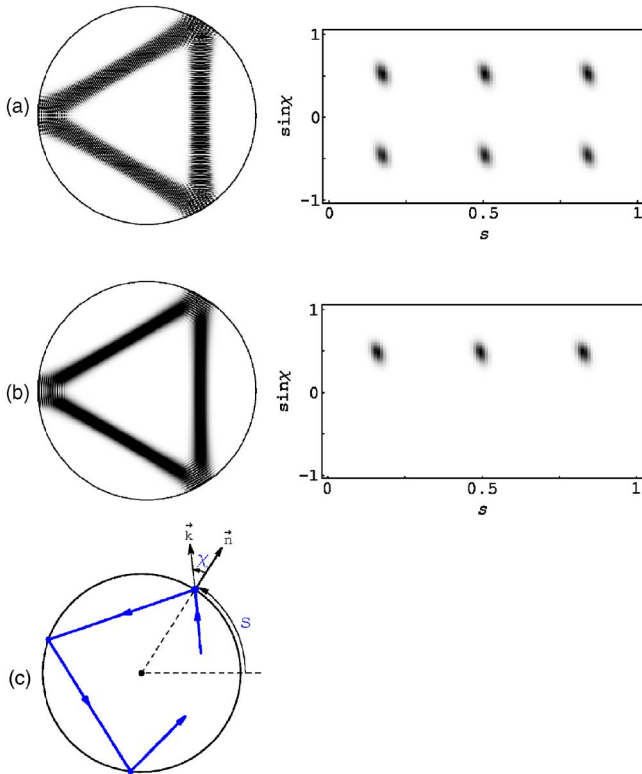
FIG. 3. (Color online) Poincaré Husimi distribution of $\Psi_{N,\ell(0)}^{p,q}(r,\phi;\theta)$ in Eq. (7) with the angular-part wave functions in the forms of (a) standing wave $\cos(\ell\phi)$ and (b) traveling wave $e^{i\ell\phi}$ and $(p,q)=(3,1)$, $\ell(0)=90$, $2N+1=21$, and $\theta=0$. (c) Motion of a particle in billiard, in which $s$ is a point on the boundary and $\chi$ is the angle of incidence with respect to the outward boundary normal.

their density plots of CSs $|\Psi_{M,\ell(0)}^{p,q}|^2$ and single eigenstates $|\psi_{n,\ell(0)}|^2$. The value of $\langle|E-\langle E\rangle|\rangle/\langle E\rangle$ decreases rapidly while $\ell(0)$ increases. At $\ell(0)\sim 60$, the value of $\langle|E-\langle E\rangle|\rangle/\langle E\rangle$ goes

to $<0.3\%$ and the plot of $|\Psi_{M,60}^{p,q}|^2$ shows much clearer localized PO than $|\Psi_{M,20}^{p,q}|^2$ and $|\Psi_{M,35}^{p,q}|^2$, so that the large quantum number $\ell(0)$ is not necessary. The density patterns of CSs $|\Psi_{M,\ell(0)}^{p,q}|^2$ and single eigenstates $|\psi_{n,\ell(0)}|^2$ are relative but totally discordant on their appearances. The eigenstates of the circular billiard $|\psi_{n,\ell(0)}|^2$, which is spreading throughout all the space, do not manifest the properties of classical POs even in the correspondence limit of large quantum numbers. However, after analytically superposing only a few of them, the wave patterns are localized on classical POs clearly. Figure 5 illustrates CSs with various parameters, in which (3, 1), (4, 1), and (5, 2) patterns are depicted at $\ell(0)=120$ and the (7, 3) one at $\ell(0)=150$. The reason of a higher $\ell(0)$ needed in the (7, 3) pattern is to satisfy that the value of $\langle|E-\langle E\rangle|\rangle/\langle E\rangle$ has to be small enough. This very effective superposition agrees very well with the previous studies in the representation of SU(2) CSs in Refs. [21–23,26–28].

## III. ROLE OF COHERENT STATES IN WEAKLY PERTURBED MESOSCOPIC SYSTEM

As stated above, the CSs related to single POs are composed of the nearly degenerate eigenstates in the ideal billiard system. In fact, the stationary quantum interference does not exist without degeneracy. Nevertheless, experimental and theoretical studies manifest that the CSs related to POs are usually to be the eigenstates in a real mesoscopic system that has the imperfection. For example, the defective structure or the deformed shape of the cavity, which is the weakly perturbation, causes the nearly degenerate eigenstates locking together and forms the localized patterns.

To produce an instance, we use a deformed circular billiard to study the properties of eigenstates in a weakly perturbed quantum system. The boundary of the deformed circular billiard is described by the function of the angular
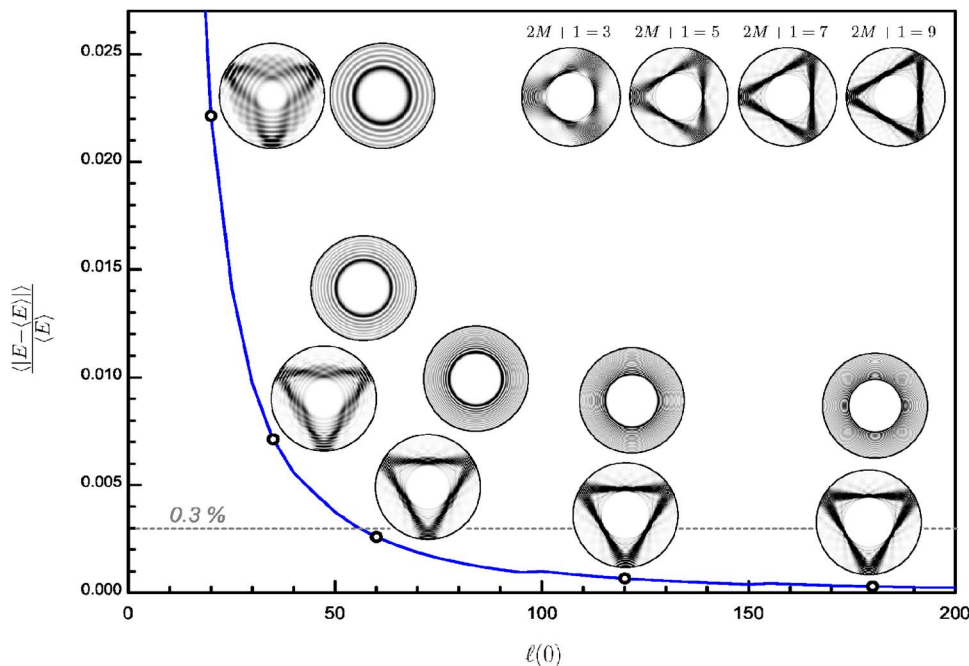


FIG. 4. (Color online) Order effects of (i) superposing number $2M+1$: At the right-up inset, four density patterns plot with different superposing numbers $2M+1=3$, 5, 7, and 9, respectively [$\ell(0)=100$, $\theta=0°$]; (ii) center angular number $\ell(0)$: Solid curve is the value of $\langle|E-\langle E\rangle|\rangle/\langle E\rangle$ and the open circles are marked at $\ell(0)=20$, 35, 60, 120, and 180 accompanying the patterns of $|\Psi_{M,\ell(0)}^{p,q}|^2$ and $|\psi_{n,\ell(0)}|^2$ ($2M+1=7$, $\theta=270°$).
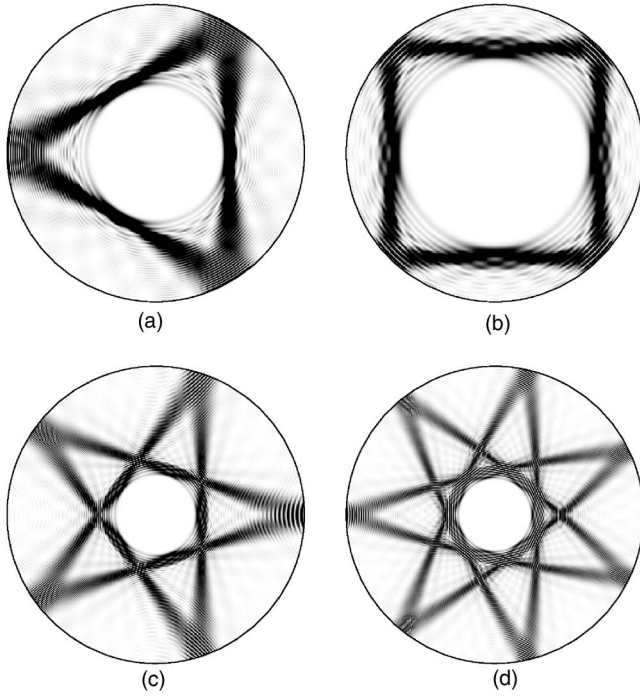
FIG. 5. The density plots of $|\Psi_{M,\ell(0)}^{p,q}(r,\phi;\theta)|^2$ for $(p,q)$ $=(3,1)$, $(4,1)$, $(5,2)$, and $(7,3)$ with $\ell(0)=120$ in (a)–(c) and $\ell(0)=150$ in (d) $(\theta=0, 2M+1=7)$.

coordinate: $r(\phi)=R\left(1+\frac{\varepsilon}{2\pi}\phi\right)$, where $\varepsilon$ is the deformation parameter and $R$ is the radius of the spiral at $\phi=0$, while the radius at $\phi=2\pi$ is $R(1+\varepsilon)$. There is a notch being created at angular origin $\phi=0$ and the deformed shape is totally asymmetric in the angular coordinate. This totally asymmetric shape is interesting to optical experiments [15,16] because of high power and directional characters concerned by the output of lasers in which their cavities are often built by semiconductors or other high-refractive index materials. Differing from these dielectric cavities, we consider the spiral-shape cavity with infinite wells and utilize the expansion method [29] to numerically calculate the eigenstates. Numerical results intriguingly reveal that the eigenstates in high-order regime are often localized on an ensemble of classical POs as shown in Fig. 6. It is clear that each eigenstate has a main localized triangle with different orientation. According to the definitions in Fig. 1, the parameters of the main localized POs in Fig. 6 are $(p,q)=(3,1)$ and their angles $\theta_{PO}$ are: (a) 75°, (b) 90°, (c) 105°, (d) 120°, (e) 135°, (f) 150°, and (g) 165°, respectively. In addition to the main triangle, there are also several lighter triangles in each pattern, for example, there is only one triangle in (a) and (g), and two or more triangles in (b)–(f). This phenomenon of multilocalized POs has also been seen in the study of the ripple billiard [30] and our result is consistent with the previous study [12]. Moreover, the experiments about weakly perturbed circular cavities also have seen the localized POs in their resonant patterns, such as the early acoustic wave patterns [13] and the optical ray trajectories [14–17].

So far we have utilized the partially CSs $|\Psi_{M,\ell(0)}^{p,q}(r,\phi;\theta)|^2$ in Eq. (8) to yield patterns with localizations on single POs overcoming that the nondegenerate states could not be al-
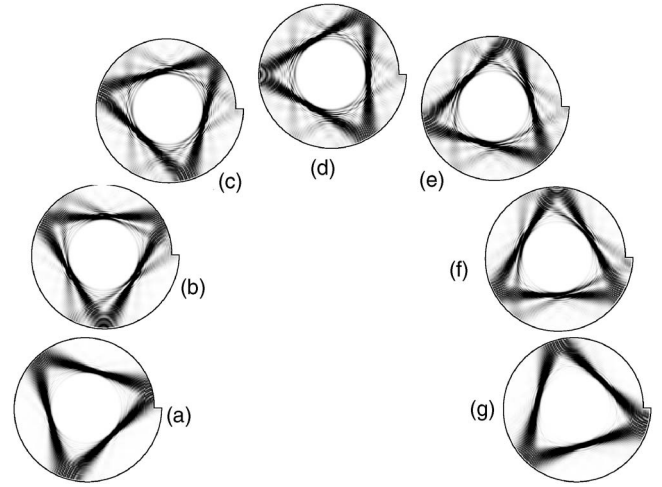


FIG. 6. Several eigenstates with localizations on POs for the spiral-shaped billiard with $\varepsilon=0.1$.

lowed to cohere to each other. However, in the perturbed mesoscopic systems, there may be more than two localized POs in each density pattern of the eigenstate as stated above. The CS in Eq. (8) is not complete enough to describe the phenomenon in the perturbed mesoscopic systems. We further extend to write down the wave function for the mesoscopic quantum systems by using the following superposition:

$$\begin{aligned}\Psi_{M,\ell(0)}^{p,q}(r,\phi;\theta_1,\theta_2,\ldots,\theta_n) &= a_1\Psi_{M,\ell(0)}^{p,q}(r,\phi;\theta_1) \\ &+ a_2\Psi_{M,\ell(0)}^{p,q}(r,\phi;\theta_2) + \cdots \\ &+ a_n\Psi_{M,\ell(0)}^{p,q}(r,\phi;\theta_n). \quad (9)\end{aligned}$$

This is the superposition of the CSs in Eq. (8), in which the values of the angles, $\theta_1$, $\theta_2,\ldots,\theta_n$ and the corresponding coefficients, $a_1$, $a_2,\ldots,a_n$, are based on the best fit to the corresponding patterns. Figure 7 shows three wave patterns obtained from Eq. (9) corresponding to eigenstates in the weakly perturbed systems, among which the first two patterns relate to the previous figures of Figs. 6(b) and 6(c) and the last one to Fig. 3(c) in Ref. [12]. These patterns are found to be excellent in agreement with their cases, and as a consequence, the wave functions in the weakly perturbed mesoscopic systems can analytically and concisely be described as the *mesoscopic eigenstate ≈ superposition of CSs*. As a correspondence of quantum mechanics and classical dynamics, the multilocalized POs of an eigenstate relate to a classical system, in which several particles are simultaneously moving on POs with different initial points.

## IV. THE VECTOR CURRENT AND THE VORTEX STRUCTURES

Vortices arising from the singular points of quantum phase can be manifest themselves and play an important role in quantum mechanics. It is of great interest to analyze the vortex behavior for the CSs in Eq. (8) by the quantum current $\vec{J}$
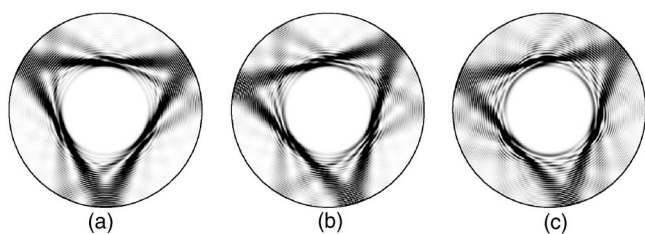
FIG. 7. Patterns superposed with several CSs relating to the eigenstates in weakly perturbed mesoscopic systems. (a) With $(\theta_1, \theta_2) = (270°, 195°)$ and $(a_1, a_2) = (0.6, -0.22)$, the pattern is similar to Fig. 6(b). (b) With $(\theta_1, \theta_2, \theta_3) = (315°, 180°, 240°)$ and $(a_1, a_2, a_3) = (0.6, -0.25, -0.06)$, the pattern is similar to Fig. 6(c). (c) Pattern superposed with $(\theta_1, \theta_2, \theta_3, \theta_4, \theta_5) = (300°, 15°, 75°, 195°, 255°)$ and $(a_1, a_2, a_3, a_4, a_5) = (0.6, 0.2, 0.2, -0.2, -0.2)$ simulate the Fig. 3(a) in Ref. [12].

$$\vec{J}(r, \phi; \theta) = \frac{\hbar}{\mu}[\text{Re } \Psi \, \nabla \, \text{Im } \Psi - \text{Im } \Psi \, \nabla \, \text{Re } \Psi]. \quad (10)$$

Figures 8(a) and 8(b) illustrate the vector current for CSs with localized $(3, 1)$ and $(5, 2)$ POs. The quantum current flown in counterclockwise direction is reflected by the billiard wall and also scattered by another current. Especially for localized POs with $q > 1$ such as $(p, q) = (5, 2)$, the magnitude and direction of the current are obviously changed at the crossing of two trajectories such as the phenomenon in classical collision of particles.

Deviating from the trajectories, the magnitudes of the current are much smaller, in particular at the region with radius $R_{\min}(p, q, \ell) = R \cos(\frac{q\pi}{p})$, the magnitudes are almost zero. The depiction of the current $\vec{J}$ is not clear enough for observing the behavior of the quantum fluctuation, and for more detailed structures one would need the normalized current $\vec{J}/|\vec{J}|$. Figures 8(c) and 8(d) show the normalized currents for CSs with localizations on $(3, 1)$ and $(5, 2)$ POs. The most characteristic of these figures is that there is a big vortex (the phase singularity) in the center of the billiard, in which the phase of the wave function is not defined. This big vortex in the circular billiard is analogous to the magnetic vortices in the superconductor type I. While the kind of superconductor type II vortices, latticelike, also can be formed in the square and triangular billiards in high-order CSs [22,23].

Figures 8(e) and 8(f) amplify the boxes in Figs. 8(c) and 8(d), in which the normalized current surrounded by the billiard wall and localized trajectories moves as disturbed flow. As we continuously amplify the patterns of the normalized current to see the fine structures, the more complex information will be visible such as singularities, saddles, and extrema (generally called critical points) corresponding to the phase fields [30,31]. These critical points (points in two dimensional space and lines in three dimensional space) play the role for realizing the fluctuation in quantum system by analyzing their spatial distribution. It has been proven that the density of the phase singularities is dependent on the frequency spectrum in random wave fields [32]. The fine structure of the normalized current in our analysis also exhibits that the density distribution of the critical points is
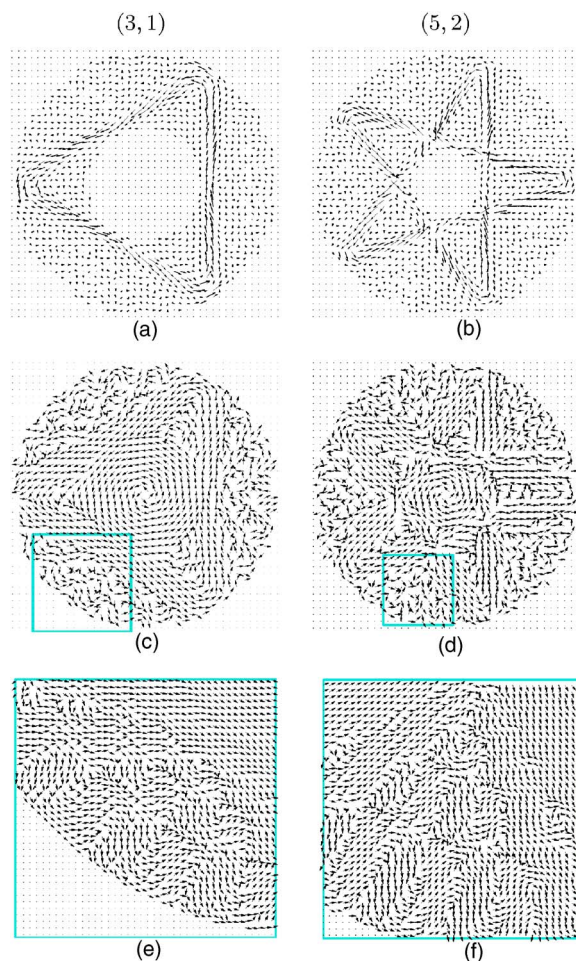


FIG. 8. (Color online) Vector current $\vec{J}$ in (a) and (b); normalized current $\vec{J}/|\vec{J}|$ in (c) and (d); (e) and (f) are the amplifications of the boxes marked in (c) and (d) ($\ell(0) = 100, 2M + 1 = 7, \theta = 0°$).

dependent on the quantum number $\ell(0)$ of the CSs sourcing from the quantum interference between the components of the CSs.

For an ideal closed system, such as the quantum billiard, the nondegenerate states are real functions; then their currents are zero and there are no vortices. The nonvanishing currents can exist when the eigenfunctions are exactly degenerate and their wave functions can be complex. However, once the ideal closed system is weakly perturbed and the exact degeneracy is lifted, the eigenfunction of the system will be all real and their currents will be zero. On the other hand, for an open system with driven excitation, such as in the laser systems, its high-order stationary states are generally found to be in terms of the superposition of nearly degenerate eigenstates, such as the present partically CSs in Eq. (8), and localized on classical POs [21,24,25]. In other words, the probability current density of the CS plays an important role in the mesoscopic stationary states of open system.

## V. CONCLUSION

We have successfully constructed wave functions related to single classical POs. We have found these wave functions

can be analytically expressed as coherent superpositions of the nearly degenerate states. Furthermore, the CSs related to single classical POs can be concisely used to represent the mesoscopic eigenstates in weakly perturbed systems and they are generally consistent with the results obtained in the previous experimental and numerical investigations [12–17]. The role of the phase factor in quantum-classical transition is clearly disclosed from the representation of quantum CSs with localizations on an ensemble of classical POs. More-over, the behavior of the vector current represent the quan-tum transport in classical limit and the formation of vortex in the normalized current is the result of quantum interference effect.

[1] M. C. Gutzwiller, *Chaos in Classical and Quantum Mechanics* (Springer-Verlag, New York, 1990), and references cited therein.

[2] M. Brack and R. K. Bhaduri, *Semiclassical Physics* (Addison-Wesley, Reading, MA, 1997), and references cited therein.

[3] H. J. Stöckmann, *Quantum Chaos: An Introduction*, (Cambridge University Press, UK, 1999), and references cited therein.

[4] R. Balian and C. Bloch, Ann. Phys. **69**, 76 (1972); M. V. Berry, Proc. R. Soc. London **413**, 183 (1987).

[5] M. A. Doncheski, S. Heppelmann, R. W. Robinett, and D. C. Tussey, Am. J. Phys. **71**, 541 (2003); R. W. Robinett and S. Heppelmann, Phys. Rev. A **65**, 062103 (2002); R. W. Robinett, Am. J. Phys. **67**, 67 (1999).

[6] B. Li and M. Robnik, J. Phys. A **28**, 2799 (1995); G. Veble, M. Robnik, and J. Liu, *ibid.* **32**, 6423 (1999); M. V. Berry, *ibid.* **10**, 2083 (1977); Philos. Trans. R. Soc. London **287**, 237 (1977).

[7] E. E. Narimanov, G. Hackenbroich, P. Jacquod, and A. D. Stone, Phys. Rev. Lett. **83**, 4991 (1999); H. E. Tureci, H. G. L. Schwefel, A. D. Stone, and E. E. Narimanov, Opt. Express **10**, 752 (2002); O. A. Starykh, P. R. J. Jacquod, E. E. Narimanov, and A. D. Stone, Phys. Rev. E **62**, 2078 (2000).

[8] A. Bäcker, S. Fürstberger, and R. Schubert, Phys. Rev. E **70**, 036204 (2004); B. Crespi, G. Perez, and S. J. Chang, *ibid.* **47**, 986 (1993).

[9] R. E. Prange, R. Narevich, and O. Zaitsev, Phys. Scr., T **90**, 134 (2001); Phys. Rev. E **59**, 1694 (1999).

[10] F. Borgonovi, G. Casati, and B. Li, Phys. Rev. Lett. **77**, 4744 (1996); K. M. Frahm and D. L. Shepelyansky, Phys. Rev. Lett. **78**, 1440 (1997).

[11] S. Y. Lee, J. W. Ryu, T. Y. Kwon, S. Rim, and C. M. Kim, Phys. Rev. A **72**, 061801(R) (2005).

[12] S. Y. Lee, S. Rim, J. W. Ryu, T. Y. Kwon, M. Choi, and C. M. Kim, Phys. Rev. Lett. **93**, 164102 (2004).

[13] P. A. Chinnery and V. F. Humphrey, Phys. Rev. E **53**, 272 (1996).

[14] J. U. Nöckel and A. D. Stone, Nature (London) **385**, 45 (1997); C. Gmachl, F. Capasso, E. E. Narimanov, J. U. Nöckel, A. D. Stone, J. Faist, D. L. Sivco, and A. Y. Cho, Science **280**, 1556 (1998); N. B. Rex, H. E. Tureci, H. G. L. Schwefel, R. K. Chang, and A. D. Stone, Phys. Rev. Lett. **88**, 094102 (2002).

[15] G. D. Chern, H. E. Tureci, A. Douglas Stone, R. K. Chang, M. Kneissl, and N. M. Johnson, Appl. Phys. Lett. **83**, 1710 (2003).

[16] T. Ben-Messaoud and J. Zyss, Appl. Phys. Lett. **86**, 241110 (2005).

[17] S. B. Lee, J. H. Lee, J. S. Chang, H. J. Moon, S. W. Kim, and K. An, Phys. Rev. Lett. **88**, 033903 (2002); T. Harayama, T. Fukushima, P. Davis, P. O. Vaccaro, T. Miyasaka, T. Nishimura, and T. Aida, Phys. Rev. E **67**, 015207(R) (2003).

[18] D. R. Tiley and J. Tiley, "*Superfluidity and Superconductivity*," 3rd ed. (Bristol, Hilger, 1990); F. Dalfovo and S. Stringari, Phys. Rev. A **53**, 2477 (1996); D. S. Rokhsar, Phys. Rev. Lett. **79**, 2164 (1997).

[19] H. Saarikoski, A. Harju, M. J. Puska, and R. M. Nieminen, Phys. Rev. Lett. **93**, 116802 (2004); K. F. Berggren, A. F. Sadreev, and A. A. Starikov, Phys. Rev. E **66**, 016218 (2002); J. R. Barker, R. Akis, and D. K. Ferry, Microelectron. Eng. **63**, 223 (2002); B. J. Baelus and F. M. Peeters, Phys. Rev. B **65**, 104515 (2002).

[20] E. Schrödinger, Naturwiss. **14**, 644 (1926).

[21] Y. F. Chen, T. H. Lu, K. W. Su, and K. F. Huang, Phys. Rev. E **72**, 056210 (2005); Y. F. Chen and K. F. Huang, J. Phys. A **36**, 7751 (2003).

[22] Y. F. Chen, K. F. Huang, and Y. P. Lan, Phys. Rev. E **66**, 046215 (2002); Y. F. Chen, K. F. Huang, and Y. P. Lan, *ibid.* **66**, 066210 (2002).

[23] Y. F. Chen and K. F. Huang, Phys. Rev. E **68**, 066207 (2003).

[24] Y. F. Chen and Y. P. Lan, Phys. Rev. A **66**, 053812 (2002); **67**, 043814 (2003).

[25] Y. F. Chen, K. F. Huang, H. C. Lai, and Y. P. Lan, Phys. Rev. E **68**, 026210 (2003).

[26] J. Pollet, O. Méplan, and C. Gignoux, J. Phys. A **28**, 7287 (1995).

[27] K. Wódkiewicz and J. H. Eberly, J. Opt. Soc. Am. B **2**, 458 (1985).

[28] V. Bužek and T. Quang, J. Opt. Soc. Am. B **6**, 2447 (1989).

[29] D. L. Kaufman, I. Kosztin, and K. Schulten, Am. J. Phys. **67**, 133 (1999).

[30] W. Li, L. E. Reichl, and B. Wu, Phys. Rev. E **65**, 056220 (2002).

[31] M. V. Berry and J. F. Nye, Nature (London) **267**, 34 (1977); J. F. Nye, *Natural Focusing and Fine Structure of Light* (Institute of Physics Publishing, Bristol and Philadelphia, 1999); I. Freund, Phys. Rev. E **52**, 2348 (1995); M. R. Dennis, Topological Singularities in Wave Fields, Ph.D. Thesis (2001).

[32] M. V. Berry and M. R. Dennis, Proc. R. Soc. London **456**, 2059 (2000); W. Wang, S. G. Hanson, Y. Miyamoto, and M. Takeda, Phys. Rev. Lett. **94**, 103902 (2005); I. Freund, J. Opt. Soc. Am. A **11**, 1644 (1994).